Vibrational Averaging of the Chemical Shift in Crystalline α-Glycine

Martin Dračínský*[a] and Petr Bouř*[a]

Averaging of the chemical shift over the molecular motion improves the simulated data and provides additional information about the temperature dependence and system dynamics. However, crystal modeling is difficult due to the limited precision of the plane-wave density functional theory (DFT) methods and approximate vibrational schemes. On the glycine example, we investigate how the averaging can be achieved within the periodic boundary conditions at the DFT level. The nuclear motion is modeled with the vibrational configuration interaction, with other simplified quantum anharmonic schemes, and the classical Born–Oppenheimer molecular dynamics (BOMD). The results confirm a large vibrational contribution to the isotropic shielding values. Both the first and second derivatives of the shielding were found important for the quantum averaging. The first derivatives influence the shielding mostly due to the anharmonic character of the CH and NH stretching modes, whereas second derivatives produce most vibrational corrections associated with the lower-frequency vibrational modes. Temperature excitations of the lowest-frequency vibrational states and the expansion of the crystal cell both determine the temperature dependence of nuclear magnetic resonance parameters. The vibrational quantum approach as well as classical BOMD schemes provided temperature dependencies of the chemical shifts that are consistent with the previous experimental data. © 2012 Wiley Periodicals, Inc.

Introduction

Glycine is intensively studied, because it is the simplest amino acid. It functions as a neurotransmitter and is one of principle components of most proteins, enzymes, and hormones. Its properties were investigated with both theoretical[1–3] and spectroscopic[4–7] methods. In the solid state, similarly as in aqueous solutions,[8] only the zwitterionic form is stable. Despite the simplicity of the molecule, crystal structures suggest that it can interact with environment in a complex way. Four polymorphic forms of solid glycine are known, referred to as α, β, γ, and δ.[9–12] The crystals of β-glycine are not stable and transform into the α or γ forms. γ-Glycine transforms into α when heated to 438 K. The α-glycine has been investigated in the temperature range 288–427 K using neutron diffraction[13]; no changes of molecular structure or phase transitions were observed under these conditions. The unit cell expands anisotropically with increasing temperature. The α-glycine crystal is formed by double layers of glycine molecules connected by hydrogen bonds.

Solid state nuclear magnetic resonance (NMR) spectra, including relaxation studies over a wide temperature range, provide valuable information about the motion of molecules and molecular groups. The insight into the structure and interactions is complementary to that provided by the diffraction methods. For example, the activation energy of 21.7 kJ/mol accompanying reorientation of the NH_3 group or the correlation time of 0.53 ns was extracted from ^1H NMR spin–lattice relaxation times measured within 173–415 K.[14] A dependence of ^{13}C and ^{15}N chemical shifts of α-glycine on temperature over the range 200–415 K was also reported but not explained. Yet, solid state NMR spectroscopy was found very useful in distinguishing polymorphs of glycine.[15] Therefore, we choose the glycine crystal as a model system to investigate the potential of the quantum chemical methods to simulate the NMR crystal vibrational averaging and temperature dependence.

The *ab initio* and density functional theory (DFT) calculations became standard interpretation tools for magnetic resonance experiments.[16,17] They are also increasingly popular for the solid state[18–23] and solutions.[24,25] Several modeling and simulation techniques have been proposed to describe the influence of the intermolecular interactions on chemical shifts. In the cluster model,[26] neighboring molecules or fragments are considered explicitly. The geometries are taken, for example, from X-ray, or neutron diffraction studies. Crystal structure of α-glycine was also modeled by the cluster method.[3]

It was soon recognized that modeling a solid as a "large molecule" or a cluster brings many difficulties. Although NMR is mostly sensitive to the local environment, for accurate computations, the long-range effects including electrostatic interactions and ring currents are significant. Therefore, the results often depended on the choice of the cluster.[27] Fortunately,

[a] M. Dračínský, P. Bouř
    Institute of Organic Chemistry and Biochemistry, Academy of Sciences,
    Flemingovo náměstí 2, Prague 166 10, Czech Republic
    E-mail: dracinsky@uochb.cas.cz
          bour@uochb.cas.cz

the translational repetition in the crystals is fully implemented in computer codes available nowadays. In the last decade, such method became popular as the gauge-including projector-augmented wave procedure (GIPAW), allowing to predict the magnetic resonance parameters.[28] Unlike the traditional methods oriented to isolated molecules, plane-wave basis set is used for GIPAW, with addition of pseudopotentials mimicking nuclear singularities. The plane-wave GIPAW approach was tested against cluster calculations, for example, for isocytosine tautomers, where the cluster modeling was clearly found inferior.[29] For various polymorphic glycine forms, the plane-wave pseudopotential methodology has been already successfully applied to produce static chemical shifts, although the static values sometimes significantly deviate (e.g., by 5 ppm for the carbonyl carbon) from experiment.[30]

The plane-wave basis offers the possibility of a fast molecular gradient computation and thus allows combining calculations of NMR parameters with molecular dynamics. Chemical shifts in the condense phase were found to be very dependent on the motional effects.[31–40] However, most computations are oriented to gas phase or solution systems. Very few examples dealing with temperature-dependent chemical shifts in the solid state are known.[33,41,42] Molecular dynamics contributes to the solvent effect in solutions, and neither it should be neglected in calculations of NMR chemical shift in crystals. In particular, in the H-bonded systems, such as the α-glycine crystal, a considerable influence of the potential energy surface anharmonicity on the shifts was predicted.[43]

The importance of the temperature or at least vibrational averaging of chemical shifts has been recognized for molecules for a long time.[44–46] Both first and second derivatives of the chemical shift with respect to the nuclear coordinates were found important for the averaging.[32] Some hydrogen vibrational corrections have been found transferable; in most cases, however, the vibrational contribution is specific and must be determined for each atom in the studied compound.[44]

In this study, several methods describing the nuclear motion are applied to α-glycine, using the plane-wave DFT within the CASTEP program for the electronic wavefunction. First, at the "quantum" approaches, crystal cell vibrations are obtained within the harmonic or anharmonic approximations, and an approximate vibrational wave function is used to average the NMR parameters. Recently, we used a similar approach to simulate vibrational properties of different quartz forms.[47] This is in principle the more advanced method. However, many approximations have to be adopted in practical computations, in particular for the treatment of the anharmonic shielding[32] and force field[48] components. The second method relies on Born–Oppenheimer molecular dynamics (BOMD) simulations[49] to sample the configurational space of the system via classical Newtonian motion of nuclei. This may miss some quantum effects; however, the direct averaging of BOMD clusters is computationally more robust than the quantum approach and may be quite appropriate for low-frequency vibrations. For both methods, the results are compared with experimental chemical shifts of α-glycine.[14] The

results confirm a large vibrational contribution to the shifts and explain at least the most important trends in the temperature dependence.

Methodology

Geometry and harmonic vibrational spectra

The starting geometries were obtained as neutron-diffraction structures from the Cambridge Crystallographic Database (codes GLYCIN20 and GLYCIN24). Using the CASTEP program,[50] atomic coordinates were optimized by energy minimization. The electron-correlation effects were modeled using the generalized gradient approximation of Perdew et al.[51] For the geometry optimization, we employed ultrasoft pseudopotentials,[52] a plane-wave cutoff energy of 340 eV, and a $3 \times 1 \times 2$ Monkhorst–Pack[53] grid to sample the Brillouin zone. The unit cell contained 40 atoms (four glycine molecules), and the lattice volume was fixed to the experimental value as obtained for the desired temperature by the neutron diffraction experiment. For control computation, a dispersion correction of the DFT functional was used[54]; this had, however, only a minor effect on the resultant chemical shifts.

Backscattered Raman and inelastic neutron scattering (INS) spectra were simulated for a crystal containing 1280 atoms. Its geometry was obtained by a $2 \times 4 \times 4$ propagation of the optimized unit cell. Computation of the larger system allowed for a partial inclusion of the delocalized crystal phonon modes.[47] The harmonic force field calculated by CASTEP was transferred on the crystal using the Cartesian tensor transfer routine,[55–57] and the Raman[58,59] and INS[60,61] intensities were obtained by usual procedures.

Backscattered Raman spectra of crystalline glycine (powder) were measured in a standard spectroscopic cell (JASCO 120-QS) with the Biotools ChiralRAMAN-2X instrument. The experimental conditions were as follows: laser wavelength 532 nm, laser power at the sample ∼20 mW, spectral resolution ∼10 cm^{-1}, and acquisition times ∼5 min. The spectrum was corrected for a fluorescence baseline.

Anharmonic averaging

To obtain the vibrational wave function, the Hamiltonian was constructed with a vibrational potential

$$V(q_1, ..., q_M) = \frac{1}{2}\sum_{i=1}^{M} \hbar\omega_i q_i^2 + \frac{1}{6}\sum_{i=1}^{M}\sum_{j=1}^{M}\sum_{k=1}^{M} c_{ijk} q_i q_j q_k$$
$$+ \frac{1}{24}\sum_{i=1}^{M}\sum_{j=1}^{M}\sum_{k=1}^{M}\sum_{l=1}^{M} d_{ijkl} q_i q_j q_k q_l, \quad (1)$$

where q_i is the dimensionless normal mode coordinate[62] i, ω_i the vibrational frequency, and c_{ijk} and d_{ijkl} (with semidiagonal "ijkk" constants only) the anharmonic cubic and quartic force field terms. Program S4[63] was used for the anharmonic computations of vibrational energies.

For the vibrational configuration interaction (VCI) the Hamiltonian was diagonalized in the harmonic oscillator basis (up to double excited states l) limited by the interaction parameter

$\left|\frac{\langle l|V|n\rangle}{E_n - E_l}\right| < 0.1$, where n is a fundamental vibration.[48] This provided 637 VCI states in total. Alternatively, degeneracy-corrected second-order perturbation method (PT2) was used.[48] Modes 1–20 (124…250 cm^{-1}) were fixed in the VCI and PT2 computations for numerical stability. Only the Γ-phonon branch[64] was considered in a crystal cell that contained four glycine molecules (number of vibrational modes $M = 3 \times N_{atoms} - 3 = 117$).

The vibrational anharmonic averaging of isotropic shielding was also performed within the S4 program environment, using the PT2 and VCI wavefunctions.[32,63] Equilibrium σ_0, first $\sigma_i = \frac{\partial \sigma}{\partial q_i}$, and diagonal second $\sigma_{ii} = \frac{\partial^2 \sigma}{\partial q_i^2}$ shielding derivatives, and the cubic and semidiagonal quartic force constants were calculated by numerical differentiation with CASTEP. The geometry (optimized, with experimental units cell parameters for each temperature of 220 and 370 K) and other computational parameters were the same as for the harmonic calculation. For the vibrational VCI or PT2 ground state j, the averaged shielding value was obtained as[32]

$$\langle \sigma \rangle_j \cong \langle j | \sigma_0 + \sum_i \sigma_i q_i + (1/2) \sum_i \sigma_{ii} q_i^2 | j \rangle \qquad (2)$$

Boltzmann average of more states was not performed because of the necessary fix of the lowest-energy modes. The remaining modes are not temperature-excited, and thus the averaging would have little effect on the final shielding.

Apart of the VCI and PT2 approaches, a third perturbational approximations was used, which is based on the harmonic oscillator limit for energies[65] and provides temperature-corrected shielding as

$$\sigma_T \cong \sigma_0 - \sum_i \frac{\sigma_i}{4\omega_i} \sum_k c_{ikk} \coth\left(\frac{\hbar\omega_k}{2kT}\right) + \sum_i \frac{\sigma_{ii}}{4} \coth\left(\frac{\hbar\omega_i}{2kT}\right).$$
$$(3)$$

This latter anharmonic terms; on the other hand, it allowed us to include also excitations of the lowest-energy vibrational modes most important for the temperature dependence of the shifts.

BOMD simulations

As for the equilibrium computations, starting geometries were based on the neutron-diffraction crystal structures of α-glycine at 301 and 427 K from the Cambridge Crystallographic Database. The structures were subjected to 96 ps BOMD[66] runs performed with the aid of the CPMD[67] software package. A time step of 0.29028 fs (12 atomic units), energy cutoff of 12.5 hartree, the BLYP[68] functional, and Vanderbilt ultrasoft pseudopotentials[52] were used in all the BOMD calculations. The default k-grid (1 × 1 × 1) was used both for the geometry optimization and for the dynamics. The temperature 300 and 427 K, respectively, was maintained with the Nosé–Hoover algorithm,[69–72] which also kept the system in the canonical "NVT" ensemble, that is, with constant number of particles (N), volume (V), and temperature (T). Trajectory snapshots were saved every 10,000 time steps (2.9 ps), and chemical shifts were calculated with the CASTEP program for each snapshot and subsequently averaged. Example of the Kohn–Sham energy variation during simulations at 300 and 427 K are given in Supporting Information, Figure S1.

Chemical shift calculations

The shielding values of the infinite glycine crystals were calculated using the CASTEP program for the optimized unit cell geometry as well as for the BOMD structures. The NMR calculations were performed using the GIPAW approach[28] at the larger cut-off option of 550 eV.[28,73] It has been verified that the results do not vary significantly for cutoffs $>\sim450$ eV. For comparison, single molecule isotropic shielding was calculated by the Gaussian program[74] at the B3LYP[68]/6-311++G** level with the default Gauge invariant atomic orbitals for the neutron diffraction geometries at 300 and 427 K, in vacuum, and within the PCM[75] solvent correction, using water dielectric parameters, as the polarity of glycine and water is similar. We use the usual notation, reserving the letter σ for isotropic shielding defined as $(\sigma_{xx} + \sigma_{yy} + \sigma_{zz})/3$, and δ for chemical shift, $\delta = \sigma_{standard} - \sigma$.

Results and Discussion

Raman and INS spectra

As discussed before,[47,76] the periodic boundary conditions enable one to obtain realistic spectral profiles for the crystal. This can also be shown in Figure 1, where the calculated INS and Raman spectra are compared to experiment. The experimental Raman spectra are somewhat affected by the baseline subtraction, which was necessary because of the fluorescence of the sample. The α-form of glycine provides a very distinct Raman intensity profile if compared to the β- and γ-forms.[30] We expect a frequency error of a few cm^{-1} both in the Raman and in the INS experiments because of the limited resolution of the spectrometers.[60,76,77]

Overall, however, the main INS and Raman experimental bands are well assignable to the predicted crystal vibrations, and the relative intensity patterns agree with the simulated intensities. Above $\sim$1720 cm^{-1}, weak INS and Raman signal not obtained by the simulation can be most probably attributed to anharmonic interactions.[78] Below 300 cm^{-1}, both Raman and INS measurements become unreliable, but also the computational model is not adequate for a real crystal, as it involves a limited number of atoms only.

On the basis of the visualization of the dynamic atomic displacement, the vibrations could be often assigned to intramolecular motions, for example, NH$_3^+$ scissoring and C=O asymmetric stretching (experimentally at $\sim$1600–1720 cm^{-1}), NH$_3^+$ twist and umbrella modes (around 1500 cm^{-1}), CH$_2$ scissoring ($\sim$1450 cm^{-1}), CH and NH bending (1316 cm^{-1}), C—N stretching and CH$_3$ wagging (1116 cm^{-1}), carbonyl carbon out of plane deviation and symmetric C=O stretching (598, 693, and 913 cm^{-1} bands), or NH$_3^+$ rotation (519 cm^{-1}). Below 500 cm^{-1}, delocalized crystal or torsional molecular modes prevail.
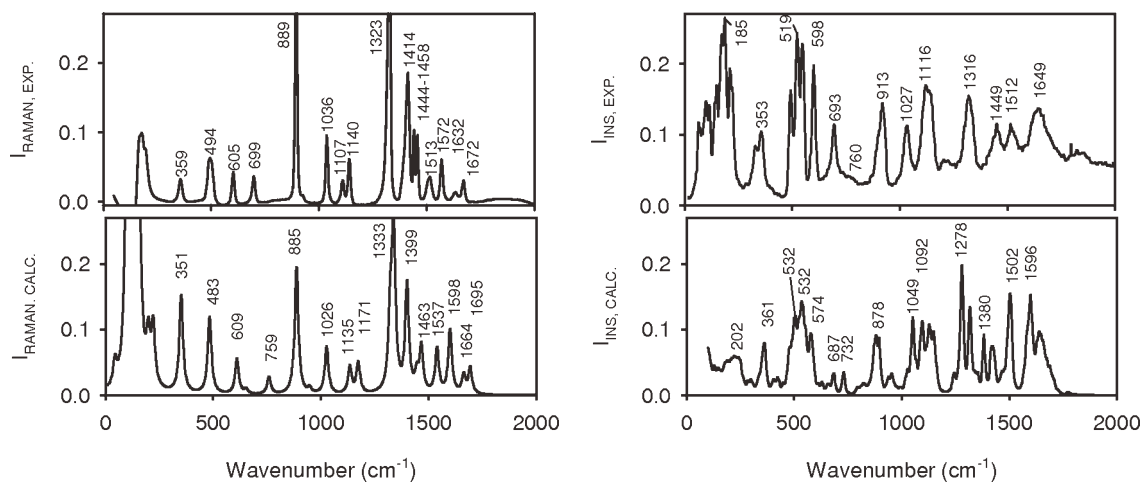
Figure 1. Experimental and calculated Raman (left) and INS (right) crystal glycine spectra. The INS spectrum is redrawn from Ref. [76]. All intensity scales are arbitrary.
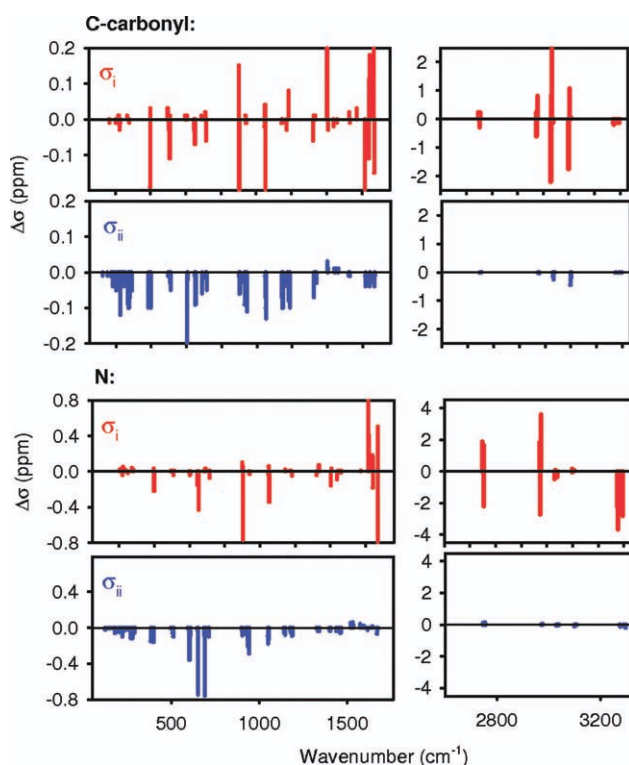
Normal mode differentiation

Due to the limited precision of the CASTEP computations, a special care had to be paid to the normal mode differentiation step used to obtain the energy and shielding derivatives. As documented at the top of Figure 2, for larger steps first derivatives of the shielding are relatively independent on the differentiation step size, but quite unreasonable shielding second derivatives were obtained for the smallest steps. The third and fourth energy derivatives (Fig. 2, bottom) are relatively stable

within normal mode steps of 0.1–0.3 a.u. The step of 0.05 is clearly too small and typically provides overestimated anharmonic force constants. Larger ($>$0.3 a.u.) steps may also lead to unrealistic constants, due to the higher-order Taylor expansion terms, not included in the potential in Eq. (1).

A more detailed analysis revealed that the errors are often caused by the lowest-frequency modes, for which even very large normal coordinate steps do not produce significant Cartesian displacements. Therefore, for further computations, the differentiations were performed in the dimensionless normal
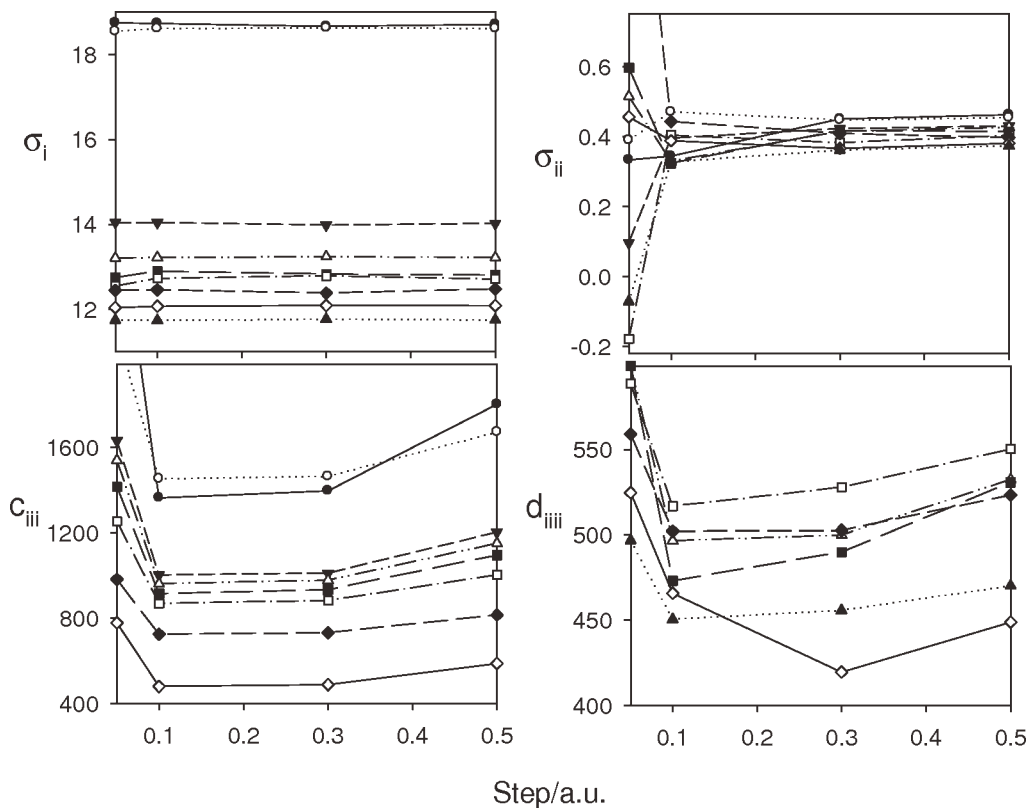
Figure 2. Dependence of the 10 largest first and second shift derivatives (in a.u., top) and third and fourth energy derivatives [c_{iii} and d_{iiii} constants in Eq. (1), in cm^{-1}, bottom] on the size of the normal mode differentiation step. Three-point ($x + \Delta$, x, $x - \Delta$) differentiation scheme was used.

Figure 3. Individual normal mode anharmonic contributions [from the first σ_i and second σ_{ii} derivatives, cf. Eq. (1), $T = 0$ K] to the carbonyl carbon (top) and nitrogen (bottom) isotropic shielding. Note the different y-scales in left and right panels.

mode coordinates[62] q_i, with a step of $q_i = \Delta Q * 1000/\omega_i$, where the normal mode differentiation step $\Delta Q = 0.5$ a.u. and ω_i is in cm^{-1}.

Anharmonic shift contributions

The first and second isotropic shielding derivatives contribute differently to the vibrational correction. This is documented in Figure 3 for the carbonyl carbon and the nitrogen atoms. The analysis is based on the perturbation computation[32] (PT2), where we can separate the first (σ_i) and second (σ_{ii}) derivative contributions as averaged over individual normal modes of the glycine crystal cell. The lower-frequency region (left part of Fig. 3) is characterized by approximately same contributions of σ_i and σ_{ii}, and below ~500 cm^{-1} the second derivatives mostly dominate. On the other hand, above 2600 cm^{-1} (right-

hand side of Fig. 3) the anharmonic shielding correction is almost entirely caused by the first derivatives.

Because the magnitude of the σ_i and σ_{ii} derivatives is about the same for all the modes, the trends in the frequency/normal mode dependence of the shifts in Figure 3 can be attributed to the force field. In particular, the high frequency modes (> 2600 cm^{-1}) comprise C—H and N—H stretching modes with a strongly anharmonic potential, which emphasize the σ_i term contributions. The rest of the modes are more harmonic in the potential; thus, only the second shielding derivatives contribute to the averaging at the harmonic potential limit. This suggests that the second shielding derivatives will be very important for the temperature effects. For 300 K, the Boltzmann quantum $kT \sim 200$ cm^{-1}, and only the lowest mode anharmonic contribution (dominated by σ_{ii}) significantly changes with the temperature. On the other hand, no rule about the total contribution of individual modes to the vibrational averaging of the crystal NMR parameters is apparent, which is consistent with previous NMR[32] and ORD[79] averaging studies. In practical computations, we thus need to consider all fundamental molecular or crystal cell vibrations.

Quantum averaging effects

Within the harmonic oscillator basis, rigorous quantum averaging of the shielding can be done. However, various methods provide slightly different results, due to the adopted approximations. The equilibrium shielding values calculated for the crystalline α-glycine atoms with the PT2, VCI [Eq. (2)], and simplified PT2 [Eq. (3)] vibrational corrections are listed in Table 1. The corrections are relatively large (even ~28% for the carbonyl ^{13}C owing to its small equilibrium shielding value) and certainly need to be considered for accurate computations.

The calculated vibrational corrections thus have the potential to improve NMR predictions; for the carbonyl chemical shift predicted recently[30] in α-glycine as 181.6 ppm a $-\Delta\sigma = -3$ ppm correction would move the results closer to experiment (176.4 ppm). However, vibrational effects in the standard may also be sizable. The computed vibrational corrections for the CH$_3$NO$_2$ molecule (Supporting Information, Table S1), which is more relevant as a standard for the glycine than TMS, are also large, in agreement with previous results for other molecules.[32,44] The temperature effects (discussed for the glycine below) in CH$_3$NO$_2$ are relatively small for ^{1}H, but quite large for ^{15}N and ^{13}C. We suppose that the temperature of the

Table 1. Computed equilibrium values of isotropic shielding σ (ppm) and their vibrational corrections ($\Delta\sigma$), for the temperature of 220 K.

Atom	σ_{Eq}	$\Delta\sigma_{PT2}$[a]	$\Delta\sigma_{VCI}$[a]	$\Delta\sigma_i$[b]	$\Delta\sigma_{ii}$[b]	$\Delta\sigma_i + \Delta\sigma_{ii}$[b]
^{13}C (CO)	−11.64	3.23	3.13	2.16	0.38	2.54
^{13}C (CH$_2$)	129.42	−5.77	−5.55	−3.93	−1.23	−5.16
^{15}N	191.59	−9.38	−9.03	−5.03	−4.28	−9.31
^{1}H (NH$_3$)[c]	21.16	−1.00	−0.95	−0.32	−0.59	−0.91
^{1}H (CH$_2$)	27.67	−0.84	−0.81	−0.66	−0.12	−0.78
^{1}H' (CH$_2$)	26.21	−0.97	−0.94	−0.72	0.15	−0.57

[a] $\Delta\sigma_{PT2}$ and $\Delta\sigma_{VCI}$—second-order perturbation and VCI calculations, involving single and double excited harmonic oscillator states, without 20 lowest-energy vibrational modes. [b] $\Delta\sigma_i$ and $\Delta\sigma_{ii}$—the second and third terms in Eq. (3). [c] Average value.

Table 2. Temperature changes in crystalline α-glycine chemical shift ($\Delta\delta = \delta_{370K} - \delta_{220K}$, in ppm), calculated by the quantum vibrational averaging.

Atom	$\Delta\delta_{Eq}$[a]	$\Delta\delta_{Eq} + \Delta\delta_{PT2}$[b]	$\Delta\delta_{Eq} + \Delta\delta_{VCI}$[b]	$\Delta\delta_{Eq} + \Delta\delta_i$[c]	$\Delta\delta_{Eq} + \Delta\delta_{ii}$[c]	$\Delta\delta_{Eq} + \Delta\delta_i + \Delta\delta_{ii}$[c]	$\Delta\delta_{Exp}$ [14]
^{13}C carbonyl	−0.12	−0.41	−0.34	−1.37	0.48	−0.78	−0.15
^{13}C methylene	−0.25	0.52	−0.30	−1.03	0.87	0.03	0.47
^{15}N	0.04	0.24	0.11	−0.36	1.17	0.76	0.80
^{1}H (NH$_3$)[c]	0.03	0.21	0.25	−0.08	0.40	0.29	∼−0.1
^{1}H (CH$_2$)	0.02	0.21	0.24	−0.05	0.44	0.37	∼0.05
^{1}H' (CH$_2$)	−0.16	−0.03	0.00	−0.29	0.27	0.15	∼−0.05

[a] Equilibrium (static) value. [b] δ_{PT2} and δ_{VCI}—PT2 and VCI calculations, as in Table 1. [c] $\Delta\delta_i$ and $\Delta\delta_{ii}$—the second and third terms in Eq. (3), corresponding to $-\Delta\sigma_i$ and $-\Delta\sigma_{ii}$.

standard was not varied in the experiment, although this is not explicitly given in Ref. [14].

The temperature-corrected terms ($\Delta\sigma_i$, $\Delta\sigma_{ii}$) add up to a value very close to the second-order perturbation correction ($\Delta\sigma_{PT2}$), which suggest that the temperature effect on the total shielding is relatively minor. This also corresponds to the analysis of individual mode contributions (Fig. 3), which indicate a decisive role of the higher-frequency vibrations not excited under usual temperatures. The VCI results correspond well to PT2. This can also be expected for relatively small nonresonant anharmonic perturbations.[48,80,81] Interestingly, the $\Delta\sigma_i$ terms are consistently larger than $\Delta\sigma_{ii}$. Thus, both the force field anharmonicities [cubic constants c_{ikk}, see Eq. (3)] and shielding derivatives (σ_i and σ_{ii}) need to be considered for reliable corrections.

The role of vibrational averaging for the temperature dependence

Although the approximations do not allow for a quantitative modeling, calculated differences in chemical shifts for two temperatures ($\delta_{370K} - \delta_{220K}$, Table 2) reveal interesting role of vibrational motions. The simulated temperatures (220 and 370 K) were chosen to lie in the most reliable interval of NMR experimental data. The $\Delta\delta_{Eq}$ differences in chemical shifts obtained for the two geometries (optimized geometries for the experimental cell dimensions at 220 and 370 K) correlate well neither with the experiment[14] nor with the vibrational averaged values.

The changes computed with the PT2 and VCI methods are clearly different from the equilibrium values and suggest a significant role of the higher-frequency vibrations during the temperature expansion of the crystal. Typically, calculated harmonic normal mode frequencies at 220 and 370 K differed by less than 0–10 cm^{-1} within the entire spectral range, that is, the influence of the geometry temperature expansion on the frequencies is minor. Unfortunately, the lowest-frequency vibrational modes most sensitive to the temperature could not be involved in PT2 or VCI computations due to the numerical instabilities and Fermi resonances.[78]

The results based on the harmonic approximation ($\Delta\delta_i + \Delta\delta_{ii}$, Table 2) thus describe the experimental trends better than PT2 and VCI. The experimental changes were very roughly estimated from the previous work.[14] Note that in particular the experimental hydrogen shift could not be estimated accurately because of signal broadening. For carbonyl ^{13}C the computation (−0.78 ppm) overestimates the experimental

value (−0.15 ppm), whereas methylene ^{13}C change (exp. 0.47 ppm) is underestimated (0.03 ppm). The ^{15}N experimental difference (0.80 ppm) is reproduced well (0.76 ppm).

Despite the errors, we thus feel that we start to understand the temperature changes in the crystal NMR. Clearly, the volume expansion and the static chemical shift values alone cannot explain the temperature dependencies. The lower-frequency vibrational motions comprised in the $\Delta\delta_i + \Delta\delta_{ii}$ terms appear as the most important contribution. The agreement of the averaging based on the harmonic approximation of the potential [Eq. (3)] with the experimental trends suggests a minor role of the quartic anharmonicities for the temperature dependence. Nevertheless, their contribution to the total shielding may be also large, as indicated by the PT2 and VCI computations (Table 1).

BOMD classical averaging

The averaging based on the Newtonian motion of nuclei was used as alternate model of the vibrational effects on the NMR shielding. The approximate span of the oxygen and hydrogen atomic positions during the 427 K BOMD is displayed on the left hand side of Figure 4. Quite similar distribution was obtained at 300 K. As apparent from Figure 4, individual molecules and functional groups oscillate around average positions and conformations, and the temperature motion results to relatively large (∼1 Å) amplitudes of individual atoms.

These deviations are larger than typical quantum uncertainties (<0.1 Å) stemming from the harmonic oscillator vibrations.[82] Also, the root means square deviations (RMSD) calculated by summing of the excited oscillator levels at 427 K are about 10 times smaller than the BOMD deviations. These RMSD were determined at the harmonic approximation as $\bar{r}_\alpha = \left(\sum_i S_{\alpha i} \frac{\omega_i}{2} \left[\exp\left(\frac{\hbar\omega_i}{kT}\right) + 1\right] / \left[\exp\left(\frac{\hbar\omega_i}{kT}\right) - 1\right]\right)^{1/2}$, α denotes the atomic coordinates, ω_i the vibrational frequency of ith vibrational mode, $S_{\alpha i}$ the normal mode-Cartesian transformation matrix, k the Boltzmann constants, and T the temperature, and are displayed as the small circles at the atomic positions on the right hand side of Figure 4. Therefore, we may suppose that the classical BOMD may tend to overestimate the temperature-related chemical shift changes. It should be noted that both the BOMD and the harmonic models involve the vibrations of the crystal cell only (Γ-branch), without the contribution of nonlocalized crystal phonon modes.

The simulated temperatures (300 and 427 K) were chosen to comprise both the neutron-scattering (geometry) and the NMR
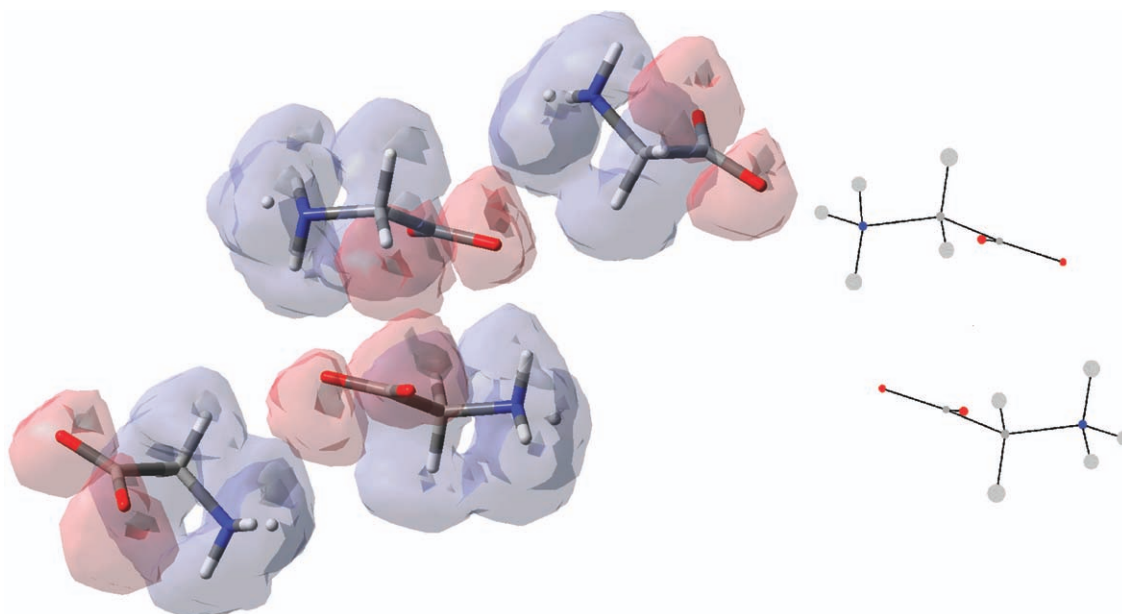
Figure 4. Left: α-glycine crystal cell, the isosurfaces indicate the maximal temperature deviations obtained as a probability isosurface of the hydrogen (gray) and oxygen (red) atoms during the BO dynamics at 427 K (300,000 geometries, ∼87 ps). Right: Harmonic quantum root mean square deviations of all atoms, displayed as the small circles, calculated at 427 K for the two middle glycine molecules.

experimental data and are slightly different than the temperature interval in the quantum modeling (220–370 K). Nevertheless, the results are well comparable because of the approximately (within the experimental error) linear dependence of the shifts on the temperature.[14] The computed shielding constants and changes in the chemical shifts are summarized in Table 3. The standard errors of the mean shielding values indicate a large shielding dispersion for individual BOMD geometries; nevertheless, the errors are smaller than the differences between the shielding values for 300 and 427 K.

The single molecule vacuum and PCM shielding (σ_{300K}, Table 3) approximately follows the values calculated for the crystal with the periodic boundary conditions. The difference (largest

for ^{13}C of CO, ∼20 ppm) can be attributed to the functional and basis set differences, including the pseudopotential in GIPAW. The PCM water correction significantly changes shieldings at the polar carbonyl and NH_3 groups (17.15 → 9.13 ppm for ^{13}C, 27.14 → 26.6 ppm for ^{1}H, Table 3). The CH_2 and perhaps surprisingly also the nitrogen are not so much affected by the environment. The calculated single molecule temperature changes ($\delta_{427K} - \delta_{300K}$) are too large and often of different sign if compared with the experiment.

The crystal computation seems to be more relevant; especially, the temperature changes computed for the optimized crystal structure are smaller than for the unoptimized geometries and closer to the experiment. The relatively large effect

Table 3. Computed equilibrium and BOMD-averaged isotropic shielding constants (σ, ppm) in glycine, and the computed and experimental temperature chemical shifts changes (δ, ppm).

	Vacuum[a]	PCM[a]	Crystal[b]	Crystal[c]	Crystal[d]	BO[e]	Exp[14]
				σ_{300K}			
^{13}C (CO)	17.15	9.13	−11.63	−11.33	−3.30	−11.0 ± 0.35	–
^{13}C (CH$_2$)	142.61	138.61	129.41	129.45	131.46	129.5 ± 0.29	–
^{15}N	206.39	206.49	191.62	192.49	194.10	187.2 ± 0.49	–
^{1}H (NH$_3$)	27.14	26.60	21.17	21.26	22.57	21.3 ± 0.05	–
^{1}H (CH$_2$)	28.43	28.38	26.26	26.32	26.80	27.3 ± 0.05	–
^{1}H′ (CH$_2$)	28.62	28.31	27.64	27.82	27.92	27.0 ± 0.06	–
				$\delta_{427K} - \delta_{300K}$			
^{13}C (CO)	−1.07	−1.23	−0.27	−0.14	−1.72	0.46	−0.20
^{13}C (CH$_2$)	−1.87	−1.9	−0.19	−0.25	−2.38	1.01	0.29
^{15}N	−6.86	−5.66	−0.06	0.00	−5.35	0.60	0.55
^{1}H (NH$_3$)	−0.64	−0.62	−0.16	−0.02	−0.74	0.12	∼−0.10
^{1}H (CH$_2$)	−0.28	−0.04	−0.28	−0.17	−0.28	0.09	∼0.05
^{1}H′ (CH$_2$)	−0.25	−0.54	−0.16	−0.05	−0.52	0.20	∼−0.05

[a] Isolated molecule, neutron diffraction geometry at a given temperature. [b] Energy minimum geometry obtained by CASTEP. [c] Energy minimum geometry obtained by CASTEP, with the dispersion correction. [54] [d] Crystal, neutron diffraction geometry. [e] Average value from 33 BOMD geometries (132 glycine molecules), with the standard error of the mean (average).

Table 4. Selected geometry parameters in α-glycine crystal.

	300 K			Change at 427 K		
	Eq.[a]	Eq.[b]	BO[c]	Eq.[a]	Eq.[b]	BO[c]
d(C=O) (Å)	1.274	1.250	1.268	−0.006	−0.005	0.004
d(C—N) (Å)	1.479	1.475	1.454	0.002	−0.002	0.008
d(N—H) (Å)	1.059	1.042	1.068	−0.004	−0.015	0.003
∠N—C—C=O (°)	158.5	161.9	177.5	−4.1	1	1.7
∠C—C—N—H (°)	57.4	58.2	60.9	0.4	2	−1.7

[a] DFT-energy minimum geometry. [b] Neutron diffraction geometry. [c] Average value from 33 raw BOMD geometries.

of optimized structure on the NMR parameters is consistent with previously reported general gradient approximation computations. For example, the 6.2, 2.0, and 2.5 ppm changes between crystal and optimized structures (Table 3, columns "crystal[b]" and "crystal[d]") reasonable agree with values of 6.2, 1.3, and 2.6 ppm found in Ref. [30], for carbonyl and methylene carbons, and nitrogen, respectively. Such isotropic shielding differences for the equilibrium crystal and DFT-optimized geometries themselves (Table 3) suggest a significant role of the vibrational motion. On the other hand, the dispersion correction[54] has a rather minor effect on the shifts and shielding, suggesting that the van der Waals forces will not be dominant in the glycine crystal. The calculated chemical shifts obtained by a linear fit between experiment and the calculation with the CASTEP minimized geometry that can be directly compared to experiment are listed in Supporting Information, Table S2. In Supporting Information, Tables S3 and S4, we list also some computed anisotropies; so far, however, no relevant experimental data are available to us, and we leave their discussion for the future.

As observed before for clusters of a solute and solvent molecules,[24] the temperature variations of the geometry cause a relatively large dispersion of the shielding values, and many clusters are required for a converged average. In our case (33 geometries), we could also average over the four glycine molecules in the elementary cell, which resulted in 132 quasi-independent values and provided a reasonably converged average shielding (Supporting Information, Fig. S2).

Selected geometry parameters are summarized in Table 4. The computations roughly reproduce the experimental trends. For example, for the equilibrium optimized structures and the 300 → 427 K temperature change, the computation predicts a 0.006 and 0.004 Å shortening of the C=O and N—H bonds, respectively. This corresponds to the experimental values for C=O and N—H (neutron diffraction geometry, 0.005 and 0.015 Å). The equilibrium C—N bond becomes larger by 0.002 Å for energy minimum geometry, although the experiment suggests a small decrease of 0.002 Å). As expected, the BO averaging leads to positive bond length changes, because of the anharmonic bond potential. Also the torsion angle changes are quite small; the largest variation of 4.1° is predicted for ∠N—C—C=O in the energy minimum geometry.

The BOMD averaging causes changes of σ_{300K} comparable with those caused by the equilibrium geometry differences. Interestingly, the chemical shift difference ($\delta_{427K} - \delta_{300K}$, Table 3) calculated by the BOMD averaging has in all cases different sign than values obtained from the differences of geometries. The geometrical differences are primarily caused by a slight temperature expansion of the crystal cell. Similarly as before (Table 2), also in the BOMD averaging the most complete model including both the lattice temperature changes and vibrational motion provides the best correlation with experiment. The ^{13}C carbonyl temperature change is not well reproduced (calculated as 0.46 ppm, experimental ∼−0.20 ppm), similarly as for the quantum methods. The experimental results suggest a very weak and possibly more complicated dependence of this atom on temperature than for the others.[14] The ^{13}C (CH$_2$) and ^{15}N chemical shift changes (calculated as 1.01 and 0.60 ppm) agree qualitatively well with the experiment (0.29 and 0.55 ppm). The hydrogen experimental shift changes are small, which is also consistent with the relatively low (<0.2 ppm) calculated temperature shift changes for these atoms.

The reasonably good agreement of the BOMD results with the observed temperature dependence and the quantum modeling are consistent with the Boltzmann-averaging concept, that is, the lowest-frequency vibrational modes are the most responsible for the chemical shift dependence as their higher-excited levels can be easily populated. The classical Newtonian dynamics for nuclei thus reproduces most of the effect. For more accurate computations, a more complete quantum temperature averaging (including both the force field and the shielding anharmonicities) is desirable. This is currently not feasible due to the time demand of the computations and may not lead to an improvement because of the limited accuracy of the applied DFT and VCI methods.

For the temperature effects, we can summarize that they are partly caused by the geometry relaxation; however, this contribution is rather minor, and the dynamics must be considered for reliable modeling. The potentially most accurate VCI method tried in this study was limited by the size of the system and limited Taylor expansion of the potential. It also did not allow performing Boltzmann weighing of lowest-energy vibrational states. However, it allowed for estimating the importance of the anharmonic potential and shielding parameters, despite some numerical errors associated with computation of the molecular property derivatives. The perturbational PT2 method in our case provided results very similar to those obtained by VCI. Finally, the approximate anharmonic formula [Eq. (3)] proved to be the best "quantum" (with respect to the treatment of nuclear motion) method for estimating the temperature trends. The classical modeling seems to be also a viable alternative, as the BOMD snapshot

averaging is quite straightforward, and the neglect of the quantum vibrational effects can be at least partially justified by the dominant role of the lowest-energy vibrational states for the temperature effects.

Despite the problems, we can conclude that the modeling including the vibrational averaging describes the main temperature changes of NMR parameters in crystal α-glycine well and helps us to better understand the dynamics and interactions of this biologically important molecule in the crystalline state.

Conclusions

To explore the performance of accurate DFT periodic boundary condition methods for the interpretation of biomolecular NMR in the crystalline phase, we included the dynamics in several ways. First, we calculated anharmonic NMR (first and second shift derivatives) and force field parameters. The numerical differentiation required more attention than for static computations on isolated molecules, because of the limited accuracy of the plane-wave method. The calculated harmonic vibrational frequencies used for the averaging provided excellent agreement with the experimental Raman and inelastic neutron scattering data. A suitable choice of the differentiation parameters enabled us to correct the equilibrium NMR parameters by the vibrational averaging and to simulate their temperature dependence. These results were in agreement with the classical BOMD model based on a direct cluster averaging.

Although the accuracy of both the NMR experiment and the computations was limited, the computed results are well consistent with the previously published experimental values. Both the first and the second NMR derivatives were found important for the temperature dependence. The temperature dependence of chemical shifts seems to be caused by multiple factors. Because of the large contribution of the lowest-frequency vibrational motions (e.g., lattice modes and NH_3 rotation) for which the BOMD averaging is appropriate, both the quantum and the classical dynamics approaches produced the most important experimentally observable trends reasonably well. The *ab initio* simulations of NMR data and crystal dynamics provide powerful means of studying molecular structure and flexibility also in the solid phase.

[1] C. H. Lin, N. Gabas, J. P. Canselier, G. Pepe, *J. Cryst. Growth* **1998**, *191,* 791.

[2] V. G. Malkin, O. L. Malkina, D. R. Salahub, *J. Am. Chem. Soc.* **1995**, *117,* 3294.

[3] A. Peeters, C. Vanalsenoy, A. T. H. Lenstra, H. J. Geise, *J. Chem. Phys.* **1995**, *103,* 6608.

[4] R. J. Appleyard, J. N. S. Evans, *J. Magn. Reson. B* **1993**, *102,* 245.

[5] S. Chongprasert, S. A. Knopp, S. L. Nail, *J. Pharm. Sci.* **2001**, *90,* 1720.

[6] R. A. Haberkorn, R. E. Stark, H. Vanwilligen, R. G. Griffin, *J. Am. Chem. Soc.* **1981**, *103,* 2534.

[7] H. Kimura, K. Nakamura, A. Eguchi, H. Sugisawa, K. Deguchi, K. Ebisawa, E. Suzuki, A. Shoji, *J. Mol. Struct.* **1998**, *447,* 247.

[8] M. Elstner, K. J. Jalkanen, M. Knapp-Mohammady, T. Frauenheim, S. Suhai, *Chem. Phys.* **2001**, *263,* 203.

[9] G. Albrecht, R. B. Corey, *J. Am. Chem. Soc.* **1939**, *61,* 1087.

[10] Y. Iitaka, *Acta Crystallogr.* **1960**, *13,* 35.

[11] Y. Iitaka, *Acta Crystallogr.* **1958**, *11,* 225.

[12] E. V. Boldyreva, S. N. Ivashevskaya, H. Sowa, H. Ahsbahs, H. P. Weber, *Z. Kristallogr.* **2005**, *220,* 50.

[13] P. Langan, S. A. Mason, D. Myles, B. P. Schoenborn, *Acta Cryst. B* **2002**, *58,* 728.

[14] R. E. Taylor, C. Dybowski, *J. Mol. Struct.* **2008**, *889,* 376.

[15] A. E. Aliev, S. E. Mann, A. S. Rahman, P. F. McMillan, F. Cora, D. Iuga, C. E. Hughes, K. D. M. Harris, *J. Phys. Chem. A* **2011**, *115,* 12201.

[16] M. Bühl, M. Kaupp, O. L. Malkina, V. G. Malkin, *J. Comput. Chem.* **1999**, *20,* 91.

[17] M. Kaupp, M. Bühl, V. G. Malkin, Calculations of NMR and EPR Parameters; Wiley-VCH: Weinheim, **2004**.

[18] G. R. Goward, D. Sebastiani, I. Schnell, H. W. Spiess, H. D. Kim, H. Ishida, *J. Am. Chem. Soc.* **2003**, *125,* 5792.

[19] R. K. Harris, S. A. Joyce, C. J. Pickard, S. Cadars, L. Emsley, *Phys. Chem. Chem. Phys.* **2006**, *8,* 137.

[20] J. Schmidt, D. Sebastiani, *J. Chem. Phys.* **2005**, *123,* 074501.

[21] C. Gervais, R. Dupree, K. J. Pike, C. Bonhomme, M. Profeta, C. J. Pickard, F. Mauri, *J. Phys. Chem. A* **2005**, *109,* 6960.

[22] J. R. Yates, T. N. Pham, C. J. Pickard, F. Mauri, A. M. Amado, A. M. Gil, S. P. Brown, *J. Am. Chem. Soc.* **2005**, *127,* 10216.

[23] J. C. Johnston, R. J. Iuliucci, J. C. Facelli, G. Fitzgerald, K. T. Mueller, *J. Chem. Phys.* **2009**, *131,* 144503.

[24] M. Dračínský, J. Kaminský, P. Bouř, *J. Phys. Chem. B* **2009**, *113,* 14698.

[25] M. Dračínský, P. Bouř, *J. Chem. Theory Comput.* **2010**, *6,* 288.

[26] R. Marek, A. Lyčka, E. Kolehmainen, E. Sievanen, J. Toušek, *Curr. Org. Chem.* **2007**, *11,* 1154.

[27] R. K. Harris, P. Hodgkinson, C. J. Pickard, J. R. Yates, V. Zorin, *Mag. Res. Chem.* **2007**, *45,* S174–S186.

[28] C. J. Pickard, F. Mauri, *Phys. Rev. B* **2001**, *6324,* 245101.

[29] M. Dračínský, P. Jansa, K. Ahonen, M. Buděšínský, *Eur. J. Org. Chem.* **2011**, *2011,* 1544.

[30] L. Stievano, F. Tielens, I. Lopes, N. Folliet, C. Gervais, D. Costa, J. C. Lambert, *Cryst. Growth Des.* **2010**, *10,* 3657.

[31] S. Tang, D. A. Case, *J. Biomol. NMR* **2007**, *38,* 255.

[32] M. Dračínský, J. Kaminský, P. Bouř, *J. Chem. Phys.* **2009**, *130,* 094106.

[33] Y. J. Lee, B. Bingol, T. Murakhtina, D. Sebastiani, W. H. Meyer, G. Wegner, H. W. Spiess, *J. Phys. Chem. B* **2007**, *111,* 9711.

[34] A. Bagno, F. D'Amico, G. Saielli, *ChemPhysChem* **2007**, *8,* 873.

[35] M. P. Waller, K. R. Geethalakshmi, M. Bühl, *J. Phys. Chem. B* **2008**, *112,* 5813.

[36] U. F. Rohrig, D. Sebastiani, *J. Phys. Chem. B* **2008**, *112,* 1267.

[37] M. Straka, P. Lantto, J. Vaara, *J. Phys. Chem. A* **2008**, *112,* 2658.

[38] J. Kongsted, C. B. Nielsen, K. V. Mikkelsen, O. Christiansen, K. Ruud, *J. Chem. Phys.* **2007**, *126,* 034510.

[39] A. J. Ilott, S. Palucha, A. S. Batsanov, M. R. Wilson, P. Hodgkinson, *J. Am. Chem. Soc.* **2010**, *132,* 5179.

[40] B. C. Mort, J. Autschbach, *J. Am. Chem. Soc.* **2006**, *128,* 10060.

[41] S. Rossano, F. Mauri, C. J. Pickard, I. Farnan, *J. Phys. Chem. B* **2005**, *109,* 7245.

[42] J. N. Dumez, C. J. Pickard, *J. Chem. Phys.* **2009**, *130,* 104701.

[43] R. Janoschek, *Mol. Phys.* **1996**, *89,* 1301.

[44] K. Ruud, P. O. Åstrand, P. R. Taylor, *J. Am. Chem. Soc.* **2001**, *123,* 4826.

[45] J. Vaara, J. Lounila, K. Ruud, T. Helgaker, *J. Chem. Phys.* **1998**, *109,* 8388.

[46] J. N. Woodford, G. S. Harbison, *J. Chem. Theory Comput.* **2006**, *2,* 1464.

[47] M. Dračínský, L. Benda, P. Bouř, *Chem. Phys. Lett.* **2011**, *512,* 5459.

[48] P. Daněček, P. Bouř, *J. Comput. Chem.* **2007**, *28,* 1617.

[49] D. Marx, J. Hutter, In Modern Methods and Algorithms of Quantum Chemistry; J. Grotendorst, Ed.; NIC: Jülich, **2000**, pp. 301–449.

[50] S. J. Clark, M. D. Segall, C. J. Pickard, P. J. Hasnip, M. J. Probert, K. Refson, M. C. Payne, *Z. Kristallogr.* **2005**, *220,* 567.

[51] J. P. Perdew, K. Burke, M. Ernzerhof, *Phys. Rev. Lett.* **1996**, *77*, 3865.

[52] D. Vanderbilt, *Phys. Rev. B* **1990**, *41*, 7892.

[53] H. J. Monkhorst, J. D. Pack, *Phys. Rev. B* **1976**, *13*, 5188.

[54] A. Tkatchenko, M. Scheffler, *Phys. Rev. Lett.* **2009**, *102,* 073005.

[55] P. Bouř, J. Sopková, L. Bednárová, P. Maloň, T. A. Keiderling, *J. Comput. Chem.* **1997**, *18,* 646.

[56] S. Yamamoto, P. Bouř, *Collect. Czech. Chem. Commun.* **2011**, *76,* 567.

[57] N. S. Bieler, M. P. Haag, C. R. Jacob, M. Reiher, *J. Chem. Theor. Comput.* **2011**, *7,* 1867.

[58] M. Buděšínský, P. Daněček, L. Bednárová, J. Kapitán, V. Baumruk, P. Bouř, *J. Phys. Chem. A* **2008**, *112,* 8633.

[59] P. L. Polavarapu, Vibrational Spectra: Principles and Applications with Emphasis on Optical Activity; Elsevier: Amsterdam, **1998**.

[60] P. Bouř, C. N. Tam, J. Sopková, F. R. Trouw, *J. Chem. Phys.* **1998**, *108,* 351.

[61] C. N. Tam, P. Bouř, J. Eckert, F. R. Trouw, *J. Phys. Chem.* **1997**, *101,* 5877.

[62] D. Papoušek, M. R. Aliev, Molecular Vibrational/Rotational Spectra; Academia: Prague, **1982**.

[63] P. Bouř, Academy of Sciences: Prague, **2010**.

[64] C. Kittel, In troduction to Solid State Physics; University of California: Berkeley, **2005**.

[65] B. C. Mort, J. Autschbach, *J. Phys. Chem. A* **2005**, *109,* 8617.

[66] R. Car, M. Parrinello, *Phys. Rev. Lett.* **1985**, *55,* 2471.

[67] CPMD V3.11 Copyright IBM Corp 1990–2006, Copyright MPI für Festkörperforschung Stuttgart, **1997**– **2001**.

[68] A. D. Becke, *J. Chem. Phys.* **1993**, *98,* 5648.

[69] W. G. Hoover, *Phys. Rev. A* **1985**, *31,* 1695.

[70] S. Nose, M. L. Klein, *Mol. Phys.* **1983**, *50,* 1055.

[71] S. Nose, *Mol. Phys.* **1984**, *52,* 255.

[72] S. Nose, *J. Chem. Phys.* **1984**, *81,* 511.

[73] J. R. Yates, C. J. Pickard, F. Mauri, *Phys. Rev. B* **2007**, *76,* 024401.

[74] M. J. Frisch, G. W. Trucks, H. B. Schlegel, G. E. Scuseria, M. A. Robb, J. R. Cheeseman, G. Scalmani, V. Barone, B. Mennucci, G. A. Petersson, H. Nakatsuji, X. Caricato, X. Li, H. P. Hratchian, A. F. Izmaylov, J. Bloino, G. Zheng, J. L. Sonnenberg, M. Hada, M. Ehara, K. Toyota, R. Fukuda, J. Hasegawa, M. Ishida, T. Nakajima, Y. Honda, O. Kitao, H. Nakai, T. Vreven, J. A. Montgomery, Jr., J. E. Peralta, F. Ogliaro, M. Bearpark, J. J. Heyd, E. Brothers, K. N. Kudin, V. N. Staroverov, R. Kobayashi, J. Normand, K. Raghavachari, A. Rendell, J. C. Burant, S. S. Iyengar, J. Tomasi, M. Cossi, N. Rega, J. M. Millam, M. Klene, J. E. Knox, J. B. Cross, V. Bakken, C. Adamo, J. Jaramillo, R. Gomperts, R. E. Stratmann, O. Yazyev, A. J. Austin, R. Cammi, C. Pomelli, J. W. Ochterski, R. L. Martin, K. Morokuma, V. G. Zakrzewski, G. A. Voth, P. Salvador, J. J. Dannenberg, S. Dapprich, A. D. Daniels, O. Farkas, J. B. Foresman, J. V. Ortiz, J. Cioslowski, D. J. Fox, Gaussian 09, Revision A.1, Gaussian, Inc.: Wallingford, CT, **2009**.

[75] G. Scalmani, M. J. Frisch, *J. Chem. Phys.* **2010**, *132*, 114110.

[76] S. F. Parker, P. I. Haris, *Spectroscopy* **2008**, *22,* 297.

[77] J. Šebestík, P. Bouř, *J. Phys. Chem. Lett.* **2011**, *2,* 498.

[78] P. Daněček, J. Kapitán, V. Baumruk, L. Bednárová, V. Kopecký, Jr., P. Bouř, *J. Chem. Phys.* **2007**, *126,* 224513.

[79] J. Kaminský, I. Raich, K. Tomčáková, P. Bouř, *J. Comp. Chem.* **2010**, *31,* 2213.

[80] V. Barone, *J. Phys. Chem. A* **2004**, *108,* 4146.

[81] M. Bounouar, C. Scheurer, *Chem. Phys.* **2008**, *347,* 194.

[82] J. Šebek, Z. Kejík, P. Bouř, *J. Phys. Chem. A* **2006**, *110,* 4702.